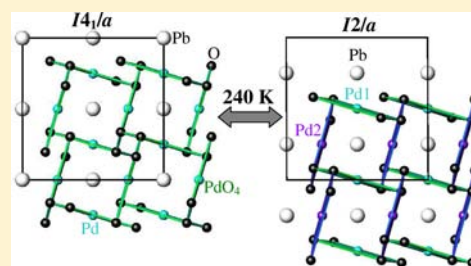


High-Pressure Synthesis, Crystal Structure, and Properties of BiPd<sub>2</sub>O<sub>4</sub> with Pd<sup>2+</sup> and Pd<sup>4+</sup> Ordering and PbPd<sub>2</sub>O<sub>4</sub>Wei Yi,<sup>†</sup> Yoshitaka Matsushita,<sup>‡</sup> Masahiko Tanaka,<sup>‡</sup> and Alexei A. Belik<sup>\*,†</sup><sup>†</sup>International Center for Materials Nanoarchitectonics (WPI-MANA), National Institute for Materials Science (NIMS), 1-1 Namiki, Tsukuba, Ibaraki 305-0044, Japan<sup>‡</sup>Spring-8 Office, National Institute for Materials Science (NIMS), Kohto 1-1-1, Sayo-cho, Hyogo 679-5148, Japan

## Supporting Information

**ABSTRACT:** BiPd<sub>2</sub>O<sub>4</sub> and PbPd<sub>2</sub>O<sub>4</sub> were synthesized at high pressure of 6 GPa and 1500 K. Crystal structures of BiPd<sub>2</sub>O<sub>4</sub> and PbPd<sub>2</sub>O<sub>4</sub> were studied with synchrotron X-ray powder diffraction. BiPd<sub>2</sub>O<sub>4</sub> is isostructural with PbPt<sub>2</sub>O<sub>4</sub> and crystallizes in a triclinic system (space group  $P\bar{1}$ ,  $a = 5.73632(4)$  Å,  $b = 6.02532(5)$  Å,  $c = 6.41100(5)$  Å,  $\alpha = 114.371(1)^\circ$ ,  $\beta = 95.910(1)^\circ$ , and  $\gamma = 111.540(1)^\circ$  at 293 K). PbPd<sub>2</sub>O<sub>4</sub> is isostructural with LaPd<sub>2</sub>O<sub>4</sub> and BaAu<sub>2</sub>O<sub>4</sub> and crystallizes in a tetragonal system (space group  $I4_1/a$ ,  $a = 5.76232(1)$  Å, and  $c = 9.98347(2)$  Å at 293 K). BiPd<sub>2</sub>O<sub>4</sub> shows ordering of Pd<sup>2+</sup> and Pd<sup>4+</sup> ions, and it is the third example of compounds with ordered arrangements of Pd<sup>2+</sup> and Pd<sup>4+</sup> in addition to Ba<sub>2</sub>Hg<sub>3</sub>Pd<sub>7</sub>O<sub>14</sub> and KPd<sub>2</sub>O<sub>3</sub>. In PbPd<sub>2</sub>O<sub>4</sub>, the following charge distribution is realized Pb<sup>4+</sup>Pd<sup>2+</sup><sub>2</sub>O<sub>4</sub>. PbPd<sub>2</sub>O<sub>4</sub> shows a structural phase transition from  $I4_1/a$  to  $I2/a$  at about 240 K keeping basically the same structural arrangements (space group  $I2/a$ ,  $a = 5.77326(1)$  Å,  $b = 9.95633(2)$  Å,  $c = 5.73264(1)$  Å,  $\beta = 90.2185(2)^\circ$  at 112 K). BiPd<sub>2</sub>O<sub>4</sub> is nonmagnetic while PbPd<sub>2</sub>O<sub>4</sub> exhibits a significant temperature-dependent paramagnetic moment of 0.46μ<sub>B</sub>/f.u. between 2 and 350 K. PbPd<sub>2</sub>O<sub>4</sub> shows metallic conductivity, and BiPd<sub>2</sub>O<sub>4</sub> is a semiconductor between 2 and 400 K.



## 1. INTRODUCTION

Compounds with the simple chemical formula ABO<sub>3</sub> crystallize in about two dozens of different structure types, for example, perovskite, LiNbO<sub>3</sub>, corundum, ilmenite (ordered corundum), hexagonal LuMnO<sub>3</sub>-type, hexagonal BaMnO<sub>3</sub>-type, pyroxene, rare earth sesquioxide structures (A, B, and C (= bixbyite)), PbReO<sub>3</sub>, KSbO<sub>3</sub>, AlFeO<sub>3</sub>, CaIrO<sub>3</sub>, cation-deficient spinel, and others.<sup>1</sup> However, “the imagination of nature” is even more unlimited in the case of compounds with the simple chemical formula AB<sub>2</sub>O<sub>4</sub>, where more than 50 individual structure types are known.<sup>2</sup> The AB<sub>2</sub>O<sub>4</sub> family includes, for example, geologically important minerals such as spinel and olivine,<sup>3</sup> the parent compound of high-temperature copper superconductors La<sub>2</sub>CuO<sub>4</sub>,<sup>4</sup> and multiferroic LuFe<sub>2</sub>O<sub>4</sub>.<sup>5</sup> The AB<sub>2</sub>O<sub>4</sub> family has also many compounds with noble metals (Ag, Au, Rh, Pt, and Pd) and unusual oxidation states of ions (Co<sup>4+</sup>, Cr<sup>6+</sup>, Cu<sup>3+</sup>, and Fe<sup>6+</sup>).<sup>2,6</sup>

In oxides, palladium usually takes oxidation states of +2 and +4.<sup>7</sup> A Pd<sup>2+</sup> ion usually has planar coordination, and it is nonmagnetic in this coordination. There are rare examples with Pd<sup>2+</sup> in octahedral coordination, for example, PdAs<sub>2</sub>O<sub>6</sub><sup>8</sup> and Ca<sub>2</sub>PdWO<sub>6</sub>,<sup>9</sup> and Pd<sup>2+</sup> can be paramagnetic in this coordination.<sup>8,10</sup> The stabilization of Pd<sup>4+</sup> requires highly oxidizing conditions (e.g., Na<sub>2</sub>PdO<sub>3</sub>)<sup>11</sup> or a high-pressure high-temperature synthetic technique (e.g., Ln<sub>2</sub>Pd<sub>2</sub>O<sub>7</sub> (Ln = Sc, In, Gd, Dy, Er, Yb, Y),<sup>12</sup> Zn<sub>2</sub>PdO<sub>4</sub>,<sup>13</sup> and Ca<sub>4</sub>PdO<sub>6</sub>).<sup>14</sup> A Pd<sup>4+</sup> ion usually has octahedral coordination.<sup>7</sup> Pd<sup>3+</sup> is rather unstable and has a strong tendency for disproportionation into Pd<sup>2+</sup> and Pd<sup>4+</sup>.

Pd<sup>3+</sup> was only found in perovskite LaPdO<sub>3</sub> in octahedral coordination.<sup>15</sup> There exist the so-called mixed-valent palladium oxides where the formal oxidation state is +2.33 (e.g., NaPd<sub>3</sub>O<sub>4</sub>)<sup>10</sup> and +2.5 (e.g., LnPd<sub>2</sub>O<sub>4</sub> (Ln = La, Pr, Nd, Gd, Y, and Lu)<sup>16–18</sup> and K<sub>3</sub>Pd<sub>2</sub>O<sub>4</sub>).<sup>11</sup> They have a tendency to keep the planar coordination of palladium ions. The charge ordering of Pd<sup>2+</sup> and Pd<sup>4+</sup> has only been observed in the Ba<sub>2</sub>Hg<sub>3</sub>Pd<sub>7</sub>O<sub>14</sub><sup>19</sup> and KPd<sub>2</sub>O<sub>3</sub><sup>20</sup> mixed-valent palladium oxides.

In this work, we added two new Pd-containing compounds to the AB<sub>2</sub>O<sub>4</sub> family: BiPd<sub>2</sub>O<sub>4</sub> and PbPd<sub>2</sub>O<sub>4</sub>. BiPd<sub>2</sub>O<sub>4</sub> shows ordering of Pd<sup>2+</sup> and Pd<sup>4+</sup> ions and seems to be the third example of compounds with ordered arrangements of Pd<sup>2+</sup> and Pd<sup>4+</sup> in addition to Ba<sub>2</sub>Hg<sub>3</sub>Pd<sub>7</sub>O<sub>14</sub><sup>19</sup> and KPd<sub>2</sub>O<sub>3</sub>.<sup>20</sup> In PbPd<sub>2</sub>O<sub>4</sub>, the following charge distribution is realized Pb<sup>4+</sup>Pd<sup>2+</sup><sub>2</sub>O<sub>4</sub>, and this compound shows a structural phase transition from  $I4_1/a$  to  $I2/a$  at 240 K (on cooling).

## 2. EXPERIMENTAL SECTION

BiPd<sub>2</sub>O<sub>4</sub> was prepared from a stoichiometric mixture of Bi<sub>2</sub>O<sub>3</sub> (99.9999%), PdO (99.9%), and KClO<sub>4</sub> (99%). PbPd<sub>2</sub>O<sub>4</sub> was prepared from a stoichiometric mixture of PbO<sub>2</sub> (99.99%) and PdO (99.9%). The mixtures were placed in Au capsules and treated at 6 GPa in a belt-type high pressure apparatus at 1500 K for 2 h (heating rate to the desired temperature was 10 min). After the heat treatment, the samples were quenched to room temperature (RT), and the pressure

Received: March 29, 2012

Published: July 3, 2012

was slowly released.  $\text{PbPd}_2\text{O}_4$  and  $\text{BiPd}_2\text{O}_4$  were black dense pellets. Both compounds were stable in air.

We also tried to synthesize  $\text{BiCu}_2\text{O}_4$ ,  $\text{PbCu}_2\text{O}_4$ ,  $\text{BiPt}_2\text{O}_4$ ,  $\text{Bi}_2\text{Pd}_2\text{O}_5$ ,  $\text{BiPdO}_3$ ,  $\text{PbPdO}_3$ ,  $\text{Bi}_2\text{RuPd}_3\text{O}_8$ ,  $\text{Bi}_2\text{IrPd}_3\text{O}_8$ , and  $\text{Bi}_2\text{PtPd}_3\text{O}_8$  at the above high-pressure high-temperature conditions. Among these compounds only  $\text{Bi}_2\text{PtPd}_3\text{O}_8$  was formed, and others were mixtures of different phases (see the Supporting Information (SI)).

X-ray powder diffraction (XRPD) data of  $\text{BiPd}_2\text{O}_4$  and  $\text{PbPd}_2\text{O}_4$  collected at RT on a RIGAKU Ultima III diffractometer using  $\text{CuK}\alpha$  radiation ( $2\theta$  range of  $10\text{--}80^\circ$ , a step width of  $0.02^\circ$ , and a counting time of 2 s/step) showed that the samples contained a small amount of PdO as an impurity, and  $\text{BiPd}_2\text{O}_4$  also contained KCl or BiOCl (depending on the sample). Synchrotron XRPD data were measured at 293 K for  $\text{BiPd}_2\text{O}_4$  and 293, 250, 230, 210, 112, and 46 K for  $\text{PbPd}_2\text{O}_4$  on a large Debye–Scherrer camera at the BL15XU beamline of SPring-8.<sup>21</sup> An  $\text{N}_2$ -gas flow system was used for the low-temperature experiment (except for 46 K where a cryostat was used), and the lowest temperature we could reach at the sample position with this system was 112 K. The intensity data were collected between  $2^\circ$  and  $60^\circ$  at the  $0.003^\circ$  interval in  $2\theta$ . The incident beam was monochromatized at  $\lambda = 0.34226 \text{ \AA}$  ( $\text{BiPd}_2\text{O}_4$ ),  $0.65297 \text{ \AA}$  ( $\text{PbPd}_2\text{O}_4$ ), and  $0.63013 \text{ \AA}$  ( $\text{PbPd}_2\text{O}_4$  at 46 K). We used the wavelength available at the time of measurements. The samples were packed into Lindenmann glass capillaries (inner diameter: 0.1 mm), which were rotated during the measurement. The absorption coefficient was measured for each sample. The Rietveld analysis was performed with RIETAN-2000.<sup>22</sup> For the impurities of PdO and BiOCl, we refined only scale factors and lattice parameters, fixing their structure parameters.

Magnetic susceptibilities ( $\chi = \text{M}/\text{H}$ ) of  $\text{BiPd}_2\text{O}_4$  and  $\text{PbPd}_2\text{O}_4$  were measured on a SQUID magnetometer (Quantum Design, MPMS) between 2 and 350 K in different applied fields under both zero-field-cooled (ZFC) and field-cooled (FC, on cooling) conditions. Isothermal magnetization measurements were performed between 0 and 50 kOe at 5 and 300 K. All the magnetization data were corrected for contributions from a diamagnetic sample holder (obtained in separate experiments) and core diamagnetism ( $\chi_{\text{dia}}/10^{-6} = -12.6 (\text{O}^{2-})$ ,  $-26 (\text{Pb}^{4+})$ ,  $-25 (\text{Bi}^{3+})$ ,  $-25 (\text{Pd}^{2+})$ , and  $-18 (\text{Pd}^{4+}) \text{ cm}^3/\text{mol}$ ).<sup>23</sup> Specific heat,  $C_p$ , was recorded between 2 and 300 K on cooling at 0 and 70 kOe by a pulse relaxation method using a commercial calorimeter (Quantum Design PPMS). dc electrical resistivity was measured between 2 and 400 K by the conventional four-probe method using a Quantum Design PPMS with the dc-gage current of 200  $\mu\text{A}$  ( $\text{PbPd}_2\text{O}_4$ ) and 1  $\mu\text{A}$  ( $\text{BiPd}_2\text{O}_4$ ). The resistivity of  $\text{BiPd}_2\text{O}_4$  was too high below about 50 K to be measured with our system. Differential scanning calorimetry (DSC) curves of  $\text{BiPd}_2\text{O}_4$  and  $\text{PbPd}_2\text{O}_4$  powders were recorded on a Mettler Toledo DSC1 STARe system at a heating/cooling rate of 2 K/min between 123 K (the lowest reachable temperature) and 300 K in open aluminum capsules. The DSC curves of  $\text{PbPd}_2\text{O}_4$  were also measured at heating/cooling rates of 10 and 20 K/min between 123 and 300 K using a large sample mass of 418.04 mg to increase the sensitivity. The density was measured using the Archimedes method using  $\text{CCl}_4$  with the density of  $1.587 \text{ g/cm}^3$ .

### 3. RESULTS AND DISCUSSION

$\text{PbPd}_2\text{O}_4$  at RT was found to be isostructural with  $\text{LnPd}_2\text{O}_4$ .<sup>16–18</sup> Therefore, we used structure parameters of  $\text{LaPd}_2\text{O}_4$ <sup>16</sup> in space group  $I4_1/a$  as the initial ones for the refinement of  $\text{PbPd}_2\text{O}_4$  using synchrotron XRPD. At 112 K, all the reflections could be indexed in space group  $I2/a$ , which is a subgroup of space group  $I4_1/a$ . Therefore, the initial structure parameters for the low-temperature phase were obtained from the  $I4_1/a$  model by lowering the symmetry to  $I2/a$ .

All the reflections (except for impurities) on the synchrotron XRPD pattern of  $\text{BiPd}_2\text{O}_4$  at RT were indexed in a triclinic system using the TREOR program.<sup>24</sup> The crystal structure of  $\text{BiPd}_2\text{O}_4$  was then solved ab initio in space group  $P\bar{1}$  (No 2)

from synchrotron XRPD data using the LeBail method<sup>25</sup> and the EXPO program.<sup>26</sup> After solving the structure of  $\text{BiPd}_2\text{O}_4$ , it was found to be isostructural with  $\text{PbPt}_2\text{O}_4$ .<sup>27,28</sup>

The refined structural parameters,  $R$  values, selected bond lengths, and bond-valence sums (BVS)<sup>29,30</sup> are listed in Tables 1–3. Experimental, calculated, and difference synchrotron

**Table 1. Structure Parameters of  $\text{PbPd}_2\text{O}_4$  at 293 and 112 K<sup>a</sup>**

site	Wyckoff position	x	y	z	B ( $\text{\AA}^2$ )
293 K <sup>b</sup>					
Pb	4a	0	0	0	0.671(6)
Pd	8d	0	0.25	0.625	0.528(8)
O	16g	0.1957(5)	0.3373(7)	0.0460(4)	0.30(7)
112 K <sup>c</sup>					
Pb	4e	0.25	0.12475(6)	0	0.034(8)
Pd1	4b	0	0.5	0	0.103(15)
Pd2	4c	0.75	0.25	0.75	0.020(15)
O1	8f	0.0810(9)	0.9224(5)	0.1895(9)	0.10(9)
O2	8f	0.5643(9)	0.6699(5)	0.8317(9)	0.15(9)

<sup>a</sup>The occupation factor ( $g$ ) of all sites is unity.  $\lambda = 0.65297 \text{ \AA}$ . <sup>b</sup>Space group  $I4_1/a$  (No 88, origin choice 1);  $Z = 4$ ;  $a = 5.76232(1) \text{ \AA}$ ,  $c = 9.98347(2) \text{ \AA}$ , and  $V = 331.4944(8) \text{ \AA}^3$ ;  $R_{\text{wp}} = 3.31\%$ ,  $R_p = 1.88\%$ ,  $R_B = 2.72\%$ , and  $R_F = 2.05\%$ ; the weight fraction of PdO is 0.3%.  $\rho_{\text{cal}} = 9.699 \text{ g/cm}^3$  and  $\rho_{\text{exp}} = 9.46(2) \text{ g/cm}^3$ . <sup>c</sup>Space group  $I2/a$  (No 15, cell choice 3);  $Z = 4$ ;  $a = 5.77326(1) \text{ \AA}$ ,  $b = 9.95633(2) \text{ \AA}$ ,  $c = 5.73264(1) \text{ \AA}$ ,  $\beta = 90.2185(2)^\circ$ , and  $V = 329.5123(11) \text{ \AA}^3$ ;  $R_{\text{wp}} = 4.55\%$ ,  $R_p = 3.00\%$ ,  $R_B = 2.93\%$ , and  $R_F = 1.25\%$ .  $\rho_{\text{cal}} = 9.757 \text{ g/cm}^3$ .

XRPD profiles are shown in Figure 1 and 2. Figures 3 and 4 show the crystal structures of  $\text{PbPd}_2\text{O}_4$  and  $\text{BiPd}_2\text{O}_4$ . There is one Pd site in  $\text{PbPd}_2\text{O}_4$  at RT, and two Pd sites in the low-temperature phase; the Pd sites have planar coordination. There are four Pd sites in  $\text{BiPd}_2\text{O}_4$ : Pd1, Pd2, and Pd3 have planar coordination, and Pd4 has octahedral coordination. The BVS values indicate the  $\text{Pd}^{2+}:\text{Pd}^{4+} = 3:1$  charge-ordering scenario in  $\text{BiPd}_2\text{O}_4$ . The BVS values of Pd1, Pd2, and Pd3 were close to +2 (from +2.07 to +2.23), and the BVS value of Pd4 was close to +4. The BVS value of Bi was close to +3 (Table 3).

One would expect  $\text{BiPd}_2\text{O}_4$  to be isostructural with  $\text{LnPd}_2\text{O}_4$  (where the formal oxidation state of Pd is +2.5, and the BVS values for Pd vary from +2.02 in  $\text{LuPd}_2\text{O}_4$  to +2.26 in  $\text{GdPd}_2\text{O}_4$ ).<sup>16–18</sup>  $\text{Pd}^{2+}$  and  $\text{Pd}^{4+}$  ( $\text{Pd}^{3+}$  is rather unstable) are statistically distributed in one crystallographic site of  $\text{LnPd}_2\text{O}_4$ . However, ordering of  $\text{Pd}^{2+}$  and  $\text{Pd}^{4+}$  takes place in  $\text{BiPd}_2\text{O}_4$ , and  $\text{BiPd}_2\text{O}_4$  adopts the structure of  $\text{PbPt}_2\text{O}_4$  with  $\text{Pd}^{4+}$  ions located in octahedral coordination.  $\text{BiPd}_2\text{O}_4$  seems to be the second compound that adopts the  $\text{PbPt}_2\text{O}_4$ -type structure.<sup>27</sup>  $\text{BiPd}_2\text{O}_4$  is also the third example of compounds with ordered arrangements of  $\text{Pd}^{2+}$  and  $\text{Pd}^{4+}$  in addition to  $\text{Ba}_2\text{Hg}_3\text{Pd}_7\text{O}_{14}$ <sup>19</sup> and  $\text{KPd}_2\text{O}_3$ .<sup>20</sup> The ‘ideal’ ordering is realized in  $\text{BiPd}_2\text{O}_4$  ( $\text{Bi}_2\text{Pd}^{4+}\text{Pd}^{2+}_3\text{O}_8$ ), and this fact could be the driving force for adopting this structure type. On the other hand, a mixed-valent state should take place in  $\text{PbPt}_2\text{O}_4$  for three sites ( $\text{Pb}^{2+}_2\text{Pt}^{4+}\text{Pt}^{2.67+}_3\text{O}_8$ ), and the driving force for such ordering is not clear. A  $\text{Bi}^{3+}$  ion has the lone electron pair; therefore, it usually has rather asymmetric coordination with 2–3 short and 2–3 long Bi–O bond lengths. This could be another reason why  $\text{BiPd}_2\text{O}_4$  does not adopt the  $\text{LnPd}_2\text{O}_4$ -type structure, where the coordination of  $\text{Ln}^{3+}$  ions is highly symmetric with four a little bit shorter and four a little bit longer equivalent

Table 2. Structure Parameters of BiPd<sub>2</sub>O<sub>4</sub> at 293 K<sup>a</sup>

site	Wyckoff position	x	y	z	B (Å <sup>2</sup> )
Bi	2i	0.13760(10)	0.75811(10)	0.35164(9)	0.586(11)
Pd1	1h	0.5	0.5	0.5	0.45(3)
Pd2	1d	0.5	0	0	0.41(2)
Pd3	1a	0	0	0	0.57(2)
Pd4	1e	0.5	0.5	0	0.31(2)
O1	2i	0.3461(13)	0.5968(15)	0.7746(13)	0.88(15)
O2	2i	0.1648(13)	0.1349(14)	0.3502(12)	0.15(13)
O3	2i	0.4843(13)	0.1482(13)	0.7632(12)	0.29(14)
O4	2i	0.1290(14)	0.3623(14)	0.0126(12)	0.79(16)

<sup>a</sup>The occupation factor (*g*) of all sites is unity.  $\lambda = 0.34226$  Å. Space group  $P\bar{1}$  (No 2);  $Z = 2$ ;  $a = 5.73632(4)$  Å,  $b = 6.02532(5)$  Å,  $c = 6.41100(5)$  Å,  $\alpha = 114.371(1)^\circ$ ,  $\beta = 95.910(1)^\circ$ ,  $\gamma = 111.540(1)^\circ$ , and  $V = 179.076(2)$  Å<sup>3</sup>;  $R_{wp} = 2.69\%$ ,  $R_p = 1.83\%$ ,  $R_B = 2.48\%$ , and  $R_F = 1.36\%$ ; the weight fraction of PdO is 0.9%, and BiOCl is 0.5%.  $\rho_{cal} = 9.010$  g/cm<sup>3</sup> and  $\rho_{exp} = 8.94(2)$  g/cm<sup>3</sup>.

Table 3. Selected Bond Lengths (*l* (Å)) and Bond Valence Sums (BVS) in BiPd<sub>2</sub>O<sub>4</sub> and PbPd<sub>2</sub>O<sub>4</sub><sup>a</sup>

PbPd <sub>2</sub> O <sub>4</sub> at 293 K			
Pb–O (×4)	2.294(4)	Pd–O (×2)	1.973(4)
Pb–O (×4)	2.509(3)	Pd–O (×2)	1.987(3)
BVS(Pb <sup>2+</sup> )	3.81	BVS(Pd <sup>2+</sup> )	2.41
BVS(Pb <sup>2+</sup> )–L	3.35	Pd–Pd	2.881
BVS(Pb <sup>4+</sup> )	3.16		
PbPd <sub>2</sub> O <sub>4</sub> at 112 K			
Pb–O2 (×2)	2.232(5)	Pd1–O2 (×2)	1.983(5)
Pb–O1 (×2)	2.244(5)	Pd1–O1 (×2)	1.998(5)
Pb–O1 (×2)	2.489(5)	BVS(Pd1 <sup>2+</sup> )	2.34
Pb–O2 (×2)	2.500(5)	Pd2–O1 (×2)	2.004(5)
BVS(Pb <sup>2+</sup> )	4.27	Pd2–O2 (×2)	2.035(5)
BVS(Pb <sup>2+</sup> )–L	3.63	BVS(Pd2 <sup>2+</sup> )	2.16
BVS(Pb <sup>4+</sup> )	3.53	Pd1–Pd2	2.887
		Pd2–Pd2	2.866
BiPd <sub>2</sub> O <sub>4</sub> at 293 K			
Bi–O2	2.222(6)	Pd2–O1 (×2)	2.009(7)
Bi–O3	2.311(6)	Pd2–O3 (×2)	2.064(6)
Bi–O4	2.317(7)	BVS(Pd2 <sup>2+</sup> )	2.07
Bi–O4	2.455(7)	Pd3–O4 (×2)	1.994(7)
Bi–O1	2.584(7)	Pd3–O2 (×2)	2.022(7)
Bi–O3	2.610(7)	BVS(Pd3 <sup>2+</sup> )	2.23
Bi–O2	2.750(6)	Pd4–O3 (×2)	1.995(6)
BVS(Bi <sup>3+</sup> )	2.84	Pd4–O1 (×2)	2.005(6)
Pd1–O1 (×2)	2.017(7)	Pd4–O4 (×2)	2.005(7)
Pd1–O2 (×2)	2.057(7)	BVS(Pd4 <sup>2+</sup> )	3.41
BVS(Pd1 <sup>2+</sup> )	2.07	BVS(Pd4 <sup>4+</sup> )	4.00

<sup>a</sup>For BVS(Pb<sup>2+</sup>)–L (L stands for the lone electron pair):  $B = 0.49$  and  $R_0(\text{Pb}^{2+}) = 1.963$ .<sup>30</sup>  $BVS = \sum_{i=1}^N \nu_i = \exp[(R_0 - l_i)/B]$ ,  $N$  is the coordination number,  $B = 0.37$ ,  $R_0(\text{Pb}^{2+}) = 2.112$ ,  $R_0(\text{Pb}^{4+}) = 2.042$ ,  $R_0(\text{Pd}^{2+}) = 1.792$ ,  $R_0(\text{Bi}^{3+}) = 2.090$ ,<sup>29</sup> and  $R_0(\text{Pd}^{4+}) = 1.851$ .<sup>19,20</sup>

Ln–O distances (e.g., 2.465 Å (×4) and 2.539 Å (×4) in LaPd<sub>2</sub>O<sub>4</sub>).<sup>16</sup>

We tried to substitute other ions, such as Ru<sup>4+</sup>, Ir<sup>4+</sup>, and Pt<sup>4+</sup> for Pd<sup>4+</sup> in BiPd<sub>2</sub>O<sub>4</sub>. However, only Bi<sub>2</sub>PtPd<sub>3</sub>O<sub>8</sub> was formed with the lattice parameters of  $a = 5.6782(2)$  Å,  $b = 6.0875(3)$  Å,  $c = 6.4227(3)$  Å,  $\alpha = 114.127(3)^\circ$ ,  $\beta = 96.352(3)^\circ$ , and  $\gamma = 111.545(3)^\circ$ . The structural analysis showed that Pd and Pt ions are statistically distributed among the four sites (see the SI). Therefore, there was no preferential substitution at the octahedral Pd4 site. The complete substitution of Pt for Pd was unsuccessful, and BiPt<sub>2</sub>O<sub>4</sub> was not formed even using a high-

pressure method. Attempts to prepare BiPt<sub>2</sub>O<sub>4</sub> at ambient pressure in the literature were also unsuccessful.<sup>28</sup>

One would expect PbPd<sub>2</sub>O<sub>4</sub> to be isostructural with PbPt<sub>2</sub>O<sub>4</sub>. However, PbPd<sub>2</sub>O<sub>4</sub> is isostructural with Ln<sup>3+</sup>Pd<sup>2.5+</sup><sub>2</sub>O<sub>4</sub><sup>16–18</sup> and Ba<sup>2+</sup>Au<sup>3+</sup><sub>2</sub>O<sub>4</sub><sup>31</sup> at RT. The BVS values<sup>29</sup> for Pb were significantly larger than +2 in PbPd<sub>2</sub>O<sub>4</sub> [BVS = +3.81 (+3.35 using different *B* and *R*<sub>0</sub> parameters for Pb<sup>2+</sup>)<sup>30</sup> at 293 K and BVS = +4.27 (+3.63) at 112 K] in comparison with the BVS value of +2.23 (+2.15) for Pb<sup>2+</sup> in PbPt<sub>2</sub>O<sub>4</sub>.<sup>27</sup> This fact suggests the Pb<sup>4+</sup> oxidation state and the charge distribution as Pb<sup>4+</sup>Pd<sup>2+</sup><sub>2</sub>O<sub>4</sub>, rather than a Pd-mixed-valent “Pb<sup>2+</sup>Pd<sup>3+</sup><sub>2</sub>O<sub>4</sub>”. Therefore, it seems that Pb<sup>2+</sup> is oxidized much easier to Pb<sup>4+</sup>, than Pd<sup>2+</sup> to Pd<sup>4+</sup>. Palladium keeps its most stable oxidation state of +2 (for oxides) in Pb<sup>4+</sup>Pd<sup>2+</sup><sub>2</sub>O<sub>4</sub> and the planar coordination. The similar situation was found in the case of perovskite PbNiO<sub>3</sub>, where lead has the oxidation state +4, and the charge distribution is Pb<sup>4+</sup>Ni<sup>2+</sup>O<sub>3</sub> because of the high stability of the Ni<sup>2+</sup> oxidation state.<sup>32</sup>

We note that the similar charge distribution could be a possibility in BiPd<sub>2</sub>O<sub>4</sub>, where ‘Bi<sup>4+</sup>’ is usually realized as Bi<sub>0.5</sub><sup>3+</sup>Bi<sub>0.5</sub><sup>5+</sup> (e.g., Bi<sub>0.5</sub><sup>3+</sup>Bi<sub>0.5</sub><sup>5+</sup>Ni<sup>2+</sup>O<sub>3</sub> and Ba<sub>2</sub>Bi<sup>3+</sup>Bi<sup>5+</sup>O<sub>6</sub>)<sup>33,34</sup>. However, in the case of BiPd<sub>2</sub>O<sub>4</sub>, it seems that Pd<sup>2+</sup> is oxidized easier to Pd<sup>4+</sup>, than Bi<sup>3+</sup> to Bi<sup>5+</sup>.

During the structural phase transition in PbPd<sub>2</sub>O<sub>4</sub> below 240 K (Figure 5b) from a tetragonal symmetry to a monoclinic symmetry, the structure keeps basically the same atomic arrangements (Figure 3). Pb<sup>4+</sup> ions are rather underbonded at RT (BVS = +3.16, Table 3) with four short and four long Pb–O bond lengths. At 112 K, all eight Pb–O bond lengths become shorter in comparison with the RT values. The shift of Pb<sup>4+</sup> ions and slight rotation of PdO<sub>4</sub> units to achieve shorter Pb–O bond lengths (and the higher BVS value of +3.53 for Pb<sup>4+</sup>, as a result) could be the driving force for the structural phase transition. A kink in volume was observed during the structural phase transition (Figure 5a).

Specific heat data of PbPd<sub>2</sub>O<sub>4</sub> and BiPd<sub>2</sub>O<sub>4</sub> plotted as *C<sub>p</sub>*/*T* versus *T* are shown in Figure 6. No anomalies were observed on the specific heat of PbPd<sub>2</sub>O<sub>4</sub>. DSC measurements also showed no anomalies when the sample weights were small. Only when we used a large sample weight for PbPd<sub>2</sub>O<sub>4</sub> and heating rates of 10 or 20 K/min we were able to detect very weak anomalies near 240 K on heating curves (Figure 5c). No anomalies were still observed on cooling curves (see the Supporting Information). The synchrotron XRPD measurements near 240 K confirmed that the DSC anomaly corresponds to a structural phase transition (Figure 5b). The temperature dependence of resistivity of PbPd<sub>2</sub>O<sub>4</sub> is depicted in

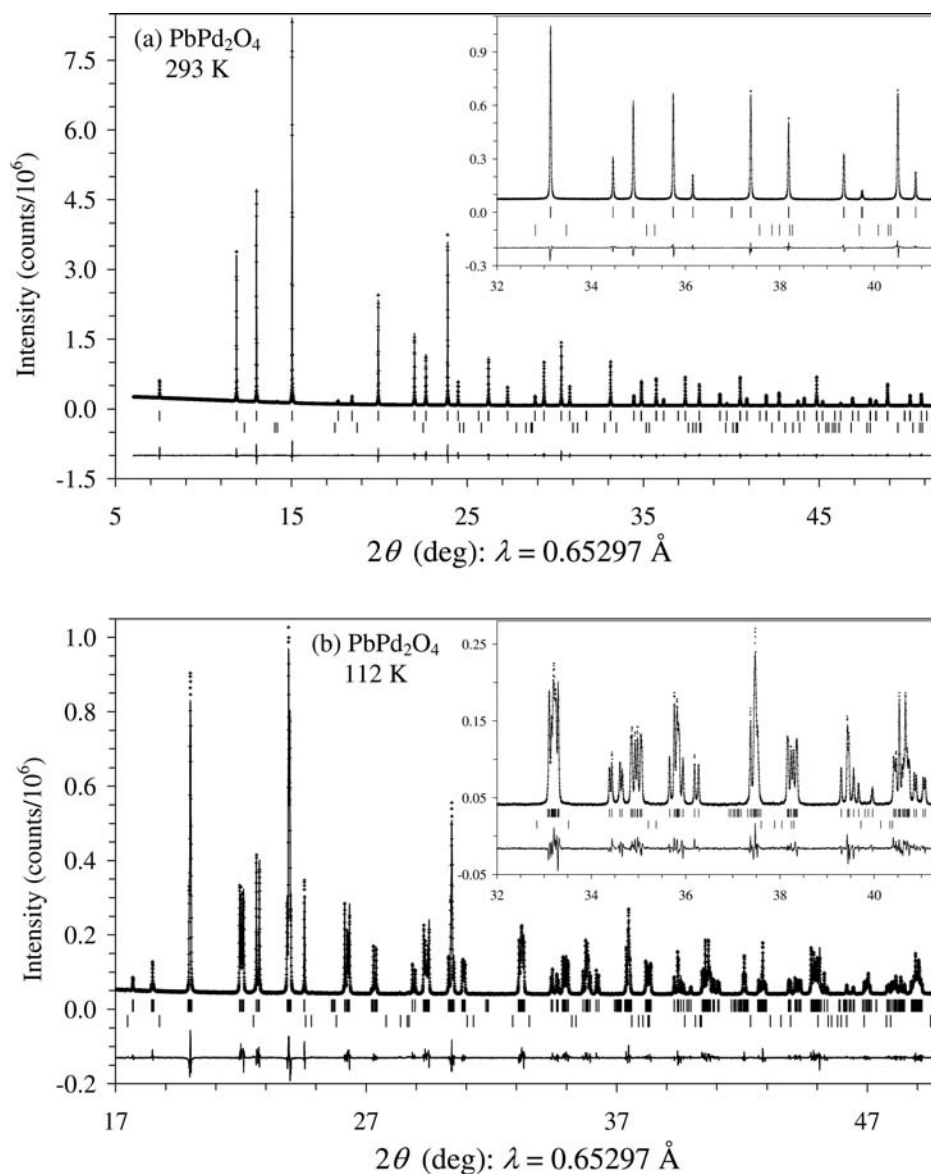


**Figure 1.** Experimental (crosses), calculated (lines), and difference synchrotron X-ray powder diffraction patterns for (a)  $\text{PbPd}_2\text{O}_4$  at 293 K and (b)  $\text{PbPd}_2\text{O}_4$  at 112 K. Bragg reflections are indicated by tick marks (the second row of tick marks is for PdO impurity). Insets show enlarged details of the figures.

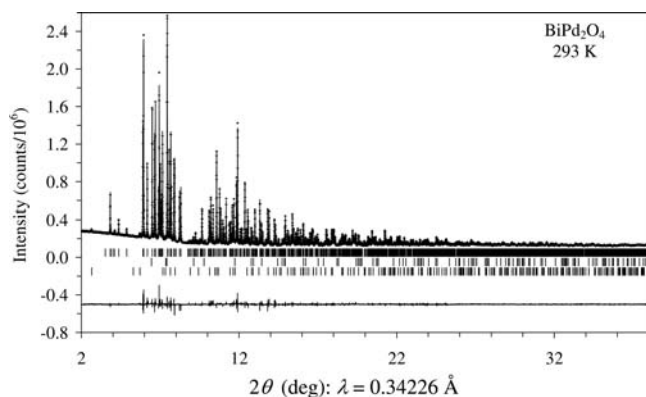


**Figure 2.** Experimental (crosses), calculated (lines), and difference synchrotron X-ray powder diffraction patterns for  $\text{BiPd}_2\text{O}_4$  at 293 K. Bragg reflections are indicated by tick marks for  $\text{BiPd}_2\text{O}_4$ , PdO, and BiOCl (from the top to the bottom).

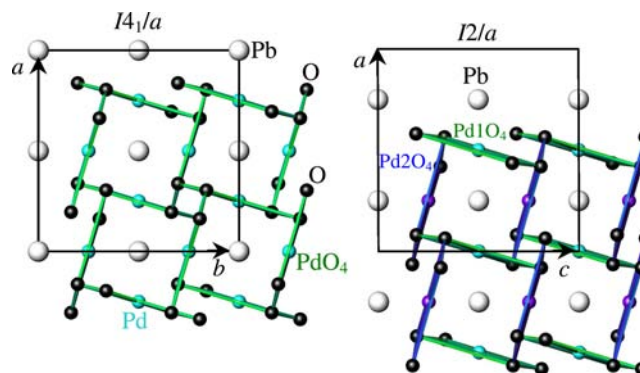


**Figure 3.** (Left) Crystal structure of  $\text{PbPd}_2\text{O}_4$  at 293 K viewed along the tetragonal  $c$  axis. (Right) Crystal structure of  $\text{PbPd}_2\text{O}_4$  at 112 K viewed along the monoclinic  $b$  axis. Pb atoms are shown by big white circles. Black circles show oxygen atoms.  $\text{PdO}_4$  planar polygons are depicted.

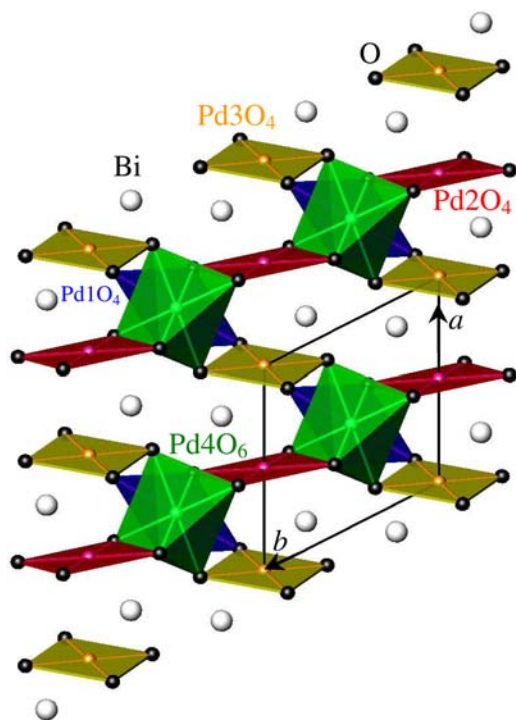


**Figure 4.** Crystal structure of  $\text{BiPd}_2\text{O}_4$  at 293 K viewed along the triclinic  $c$  axis. Bi atoms are shown by big white circles. Black circles show oxygen atoms.  $\text{PdO}_4$  planar polygons and  $\text{Pd}_4\text{O}_6$  octahedra are depicted.

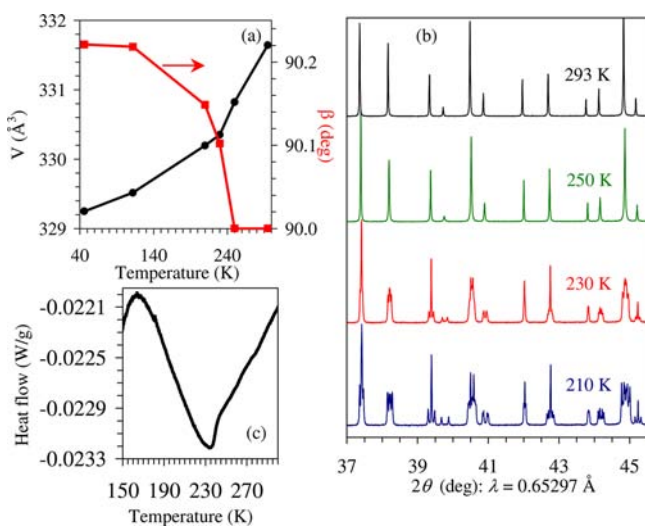


**Figure 5.** (a) Temperature dependence of the unit cell volume and monoclinic angle  $\beta$  in  $\text{PbPd}_2\text{O}_4$ . (b) Fragments of synchrotron X-ray powder diffraction patterns of  $\text{PbPd}_2\text{O}_4$  at 293, 250, 230, and 210 K. (c) A fragment of the differential scanning calorimetry curve of  $\text{PbPd}_2\text{O}_4$  (418.04 mg) measured at a heating rate of 10 K/min from 123 to 293 K.

Figure 6a.  $\text{PbPd}_2\text{O}_4$  shows metallic resistivity with a kink near 240 K. The electronic contribution ( $\gamma$ ) to the specific heat was estimated to be  $24.2 \text{ mJ}\cdot\text{mol}^{-1}\cdot\text{K}^{-2}$  (from the low-temperature fit of the  $C_p/T$  vs  $T^2$  data) which is comparable with that of some metals, for example,  $\gamma = 6.54 \text{ mJ}\cdot\text{mol}^{-1}\cdot\text{K}^{-2}$  for Pt.<sup>35</sup> There were no anomalies on specific heat and DSC curves of  $\text{BiPd}_2\text{O}_4$  indicating the absence of low-temperature phase transitions (Figure 6b). Temperature dependence of resistivity

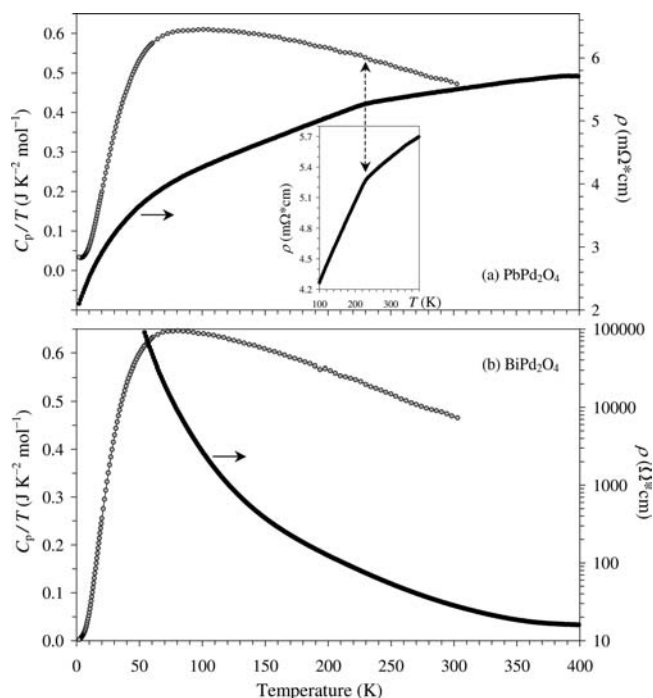


**Figure 6.** (a) Specific heat data plotted as  $C_p/T$  versus  $T$  (the left-hand axis) and temperature dependence of resistivity (the right-hand axis) of  $\text{PbPd}_2\text{O}_4$ . The vertical double arrow shows the structural phase transition temperature. The inset depicts a fragment of the resistivity curve. (b) Specific heat data (the left-hand axis) and temperature dependence of resistivity (the right-hand axis) of  $\text{BiPd}_2\text{O}_4$ .

of  $\text{BiPd}_2\text{O}_4$  showed that it is a semiconductor. There was a negligible electronic contribution to the specific heat of  $\text{BiPd}_2\text{O}_4$  (see the SI) in agreement with its semiconducting nature.

Figure 7 shows the  $\chi$  versus  $T$  curves of  $\text{PbPd}_2\text{O}_4$  and  $\text{BiPd}_2\text{O}_4$  at 50 kOe and  $M$  versus  $H$  curves. No anomalies on the magnetic susceptibilities could be seen in  $\text{PbPd}_2\text{O}_4$  around 240 K. There was basically no difference between the ZFC and FC curves. Note that very weak anomalies near 50 K on the FC curves could originate from a ferromagnetic impurity. However, the  $M$  versus  $H$  curves were linear from the origin indicating that a ferromagnetic contribution is very small. The ZFC susceptibility curves were fit with the modified Curie–Weiss equation

$$\chi(T) = \chi_0 + \mu_{\text{eff}}^2 N(3k_{\text{B}}(T - \theta))^{-1} \quad (1)$$

where  $\chi_0$  is the temperature independent term,  $\mu_{\text{eff}}$  is the effective magnetic moment,  $N$  is Avogadro's number,  $k_{\text{B}}$  is Boltzmann's constant, and  $\theta$  is the Weiss constant. The fitting parameters were  $\chi_0 = 5.48(2) \times 10^{-5} \text{ cm}^3\cdot\text{mol}^{-1}$ ,  $\mu_{\text{eff}} = 0.0807(3)\mu_{\text{B}}/\text{f.u.}$ , and  $\theta = -1.50(3) \text{ K}$  for  $\text{BiPd}_2\text{O}_4$  (the  $\chi$  vs  $T$  curve was fit; Figure 7a) and  $\chi_0 = 1.170(5) \times 10^{-4} \text{ cm}^3\cdot\text{mol}^{-1}$ ,  $\mu_{\text{eff}} = 0.457(1)\mu_{\text{B}}/\text{f.u.}$ , and  $\theta = -14.4(2) \text{ K}$  for  $\text{PbPd}_2\text{O}_4$  (the  $\chi^{-1}$  vs  $T$  curve was fit; Figure 7a). The fitting parameters in  $\text{BiPd}_2\text{O}_4$  suggest that its magnetism comes from traces of paramagnetic impurities.  $\text{BiPd}_2\text{O}_4$  is nonmagnetic, and this is in agreement with the nonmagnetic ground states of  $\text{Pd}^{2+}$  ( $d^8$ ) ions in planar coordination and  $\text{Pd}^{4+}$  ( $d^6$  or  $t_{2g}^6$ ) ions. The significant temperature-dependent paramagnetic moment of  $0.457\mu_{\text{B}}/\text{f.u.}$  in  $\text{PbPd}_2\text{O}_4$  is too large to be assigned to impurities or defects. This fact indicates that the sample has a

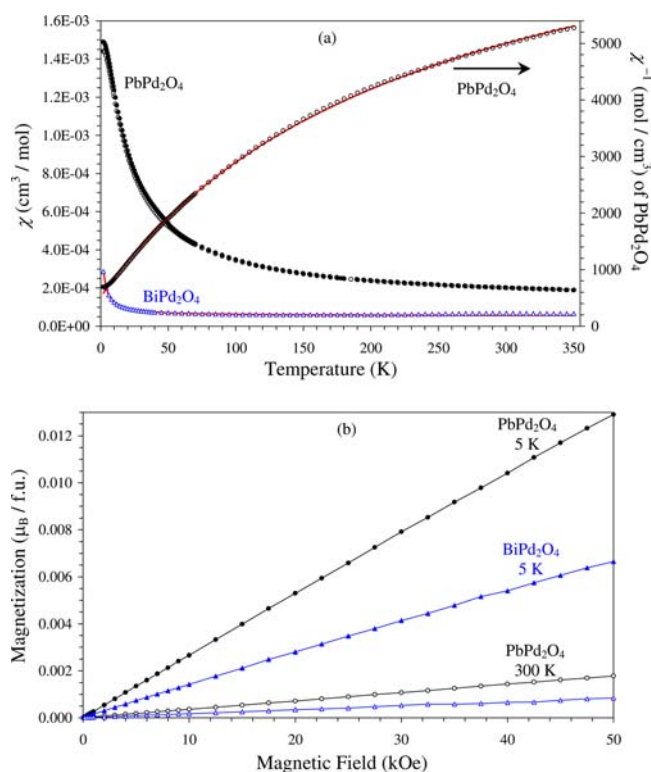


**Figure 7.** (a) ZFC (white symbols) and FC (black symbols) dc magnetic susceptibility ( $\chi = M/H$ ) curves of  $\text{PbPd}_2\text{O}_4$  (circles) and  $\text{BiPd}_2\text{O}_4$  (triangles; only the ZFC curve is shown) at 50 kOe. The right-hand axis gives the ZFC  $\chi^{-1}$  vs  $T$  curve for  $\text{PbPd}_2\text{O}_4$ . The red line shows fitting results with eq 1. (b) Isothermal magnetization curves of  $\text{PbPd}_2\text{O}_4$  (circles) and  $\text{BiPd}_2\text{O}_4$  (triangles) at 5 K (filled symbols) and 300 K (white symbols).

significant fraction of unpaired electrons, which can be responsible for its metallic behavior.

$\text{LnPd}_2\text{O}_4$  ( $\text{Ln} = \text{La}, \text{Pr}, \text{Nd}, \text{Gd}, \text{and Y}$ ) compounds are semiconductors with the Pd–Pd distances varying from 2.951 Å ( $\text{Ln} = \text{La}$ )<sup>16</sup> to 2.868 Å ( $\text{Ln} = \text{Y}$ )<sup>17</sup> to 2.840 Å ( $\text{Ln} = \text{Lu}$ ).<sup>18</sup> On the other hand,  $\text{PbPd}_2\text{O}_4$  with the Pd–Pd distance of 2.881 Å (at RT) shows metallic conductivity between 2 and 400 K. The Pd–Pd distances split into 2.866 and 2.887 Å (at 112 K). Therefore, electronic states of palladium in  $\text{LnPd}_2\text{O}_4$  and  $\text{PbPd}_2\text{O}_4$  should be crucial for their different electronic properties, not the Pd–Pd distances.

Actually electronic and magnetic properties of both  $\text{LnPd}_2\text{O}_4$  and  $\text{PbPd}_2\text{O}_4$  are different from naïve expectation. For the mixed-valent  $\text{Ln}^{3+}\text{Pd}^{2.5+}_2\text{O}_4$ , one would expect metallic conductivity, while a semiconducting behavior would be expected for localized nonmagnetic  $\text{Pd}^{2+}$  (and  $\text{Pd}^{4+}$ ) systems (as it was observed in  $\text{BiPd}_2\text{O}_4$ ).  $\text{LnPd}_2\text{O}_4$  shows semiconducting behavior experimentally; therefore, temperature-dependent paramagnetic properties would be expected. However,  $\text{LaPd}_2\text{O}_4$  exhibits temperature-independent paramagnetism with an experimental susceptibility of  $2.72 \times 10^{-4} \text{ cm}^3/\text{mol}$  (cf., an experimental susceptibility of  $\text{PbPd}_2\text{O}_4$  at 300 K is  $2.02 \times 10^{-4} \text{ cm}^3/\text{mol}$ ).<sup>16</sup> On the other hand, metallic  $\text{PbPd}_2\text{O}_4$  should show temperature-independent Pauli paramagnetism, while it exhibits a temperature-dependent paramagnetic moment. It is possible that the oxygen and cation nonstoichiometry plays a significant role in  $\text{LnPd}_2\text{O}_4$  and  $\text{PbPd}_2\text{O}_4$ . The experimental density of  $\text{PbPd}_2\text{O}_4$  (Table 1) corresponds to the composition of  $\text{Pb}_{0.975}\text{Pd}_{1.95}\text{O}_4$ . However,

the reliable structural refinement of occupation factors ( $g$ ) was difficult because of the strong correlation among  $g(\text{Pb})$ ,  $g(\text{Pd})$ , and  $B(\text{O})$ . More experimental and theoretical work will be needed to understand physical properties of  $\text{LnPd}_2\text{O}_4$  and  $\text{PbPd}_2\text{O}_4$ .

In conclusion, we prepared two new members of the  $\text{AB}_2\text{O}_4$  family:  $\text{BiPd}_2\text{O}_4$  and  $\text{PbPd}_2\text{O}_4$  by a high-pressure high-temperature method. The following charge distributions are realized in them,  $\text{Bi}^{3+}_2\text{Pd}^{4+}\text{Pd}^{2+}_3\text{O}_8$  and  $\text{Pb}^{4+}\text{Pd}^{2+}_2\text{O}_4$ .  $\text{BiPd}_2\text{O}_4$  is the third example of compounds with ordered arrangements of  $\text{Pd}^{2+}$  and  $\text{Pd}^{4+}$  ions in addition to  $\text{Ba}_2\text{Hg}_3\text{Pd}_7\text{O}_{14}$ <sup>19</sup> and  $\text{KPd}_2\text{O}_3$ .<sup>20</sup>  $\text{BiPd}_2\text{O}_4$  is isostructural with  $\text{PbPt}_2\text{O}_4$ , and  $\text{PbPd}_2\text{O}_4$  with  $\text{LaPd}_2\text{O}_4$  and  $\text{BaAu}_2\text{O}_4$ .

## ■ ASSOCIATED CONTENT

### Supporting Information

SXRD patterns of  $\text{BiPd}_2\text{O}_4$  with  $\lambda = 0.65297$  Å, phase compositions of samples with the total compositions of  $\text{BiCu}_2\text{O}_4$ ,  $\text{PbCu}_2\text{O}_4$ ,  $\text{BiPt}_2\text{O}_4$ ,  $\text{Bi}_2\text{Pd}_2\text{O}_5$ ,  $\text{BiPdO}_3$ ,  $\text{PbPdO}_3$ ,  $\text{Bi}_2\text{RuPd}_3\text{O}_8$ ,  $\text{Bi}_2\text{IrPd}_3\text{O}_8$ , and  $\text{Bi}_2\text{PtPd}_3\text{O}_8$ ; structure parameters and magnetic data of  $\text{Bi}_2\text{PtPd}_3\text{O}_8$ ; the DSC, specific heat, and magnetization data for  $\text{PbPd}_2\text{O}_4$  and  $\text{BiPd}_2\text{O}_4$  (PDF). This material is available free of charge via the Internet at <http://pubs.acs.org>.

## ■ AUTHOR INFORMATION

### Corresponding Author

\*To whom all correspondence should be addressed. E-mail: Alexei.Belik@nims.go.jp.

### Notes

The authors declare no competing financial interest.

## ■ ACKNOWLEDGMENTS

This work was supported by World Premier International Research Center Initiative (WPI Initiative, MEXT, Japan), the Japan Society for the Promotion of Science (JSPS) through its “Funding Program for World-Leading Innovative R&D on Science and Technology (FIRST Program)”, and the Grants-in-Aid for Scientific Research (22246083) from JSPS, Japan. The synchrotron radiation experiments were performed at the SPring-8 with the approval of the Japan Synchrotron Radiation Research Institute (Proposal Number: 2011B4512).

## ■ REFERENCES

- (1) (a) Giaquinta, D. M.; zur Loye, H.-C. *Chem. Mater.* **1994**, *6*, 365. (b) Bharathy, M.; Fox, A. H.; Mugavero, S. J.; zur Loye, H.-C. *Solid State Sci.* **2009**, *11*, 651.
- (2) Müller-Buschbaum, Hk. *J. Alloy. Compd.* **2003**, *349*, 49.
- (3) Zhang, S. Q.; Karato, S. *Nature* **1995**, *375*, 774.
- (4) Anderson, P. W. *Science* **1987**, *235*, 1196.
- (5) Ikeda, N.; Ohsumi, H.; Ohwada, K.; Ishii, K.; Inami, T.; Kakurai, K.; Murakami, Y.; Yoshii, K.; Mori, S.; Horibe, Y.; Kito, H. *Nature* **2005**, *436*, 1136.
- (6) Audette, R. J.; Quail, J. W.; Black, W. H.; Robertson, B. E. *J. Solid State Chem.* **1973**, *8*, 43.
- (7) Müller-Buschbaum, Hk. *Z. Anorg. Allg. Chem.* **2005**, *631*, 239.
- (8) Orosel, D.; Jansen, M. *Z. Anorg. Allg. Chem.* **2006**, *632*, 1131.
- (9) Fu, Z. M.; Li, W. X. *Sci. China* **1996**, *A39*, 981.
- (10) Reehuis, M.; Saha-Dasgupta, T.; Orosel, D.; Nuss, J.; Rahaman, B.; Keimer, B.; Andersen, O. K.; Jansen, M. *Phys. Rev. B* **2012**, *85*, 115118.
- (11) Panin, R. V.; Khasanova, N. R.; Abakumov, A. M.; Antipov, E. V.; Van Tendeloo, G.; Schnelle, W. *J. Solid State Chem.* **2007**, *180*, 1566.

- (12) Sleight, A. W. *Mater. Res. Bull.* **1968**, *3*, 699.
- (13) Demazeau, G.; Omeran, I.; Pouchard, M.; Hagenmuller, P. *Mater. Res. Bull.* **1976**, *11*, 1449.
- (14) Wang, Y.-H.; Walker, D.; Chen, B.-H.; Scott, B. A. *J. Alloy. Compd.* **1999**, *285*, 98.
- (15) Kim, S.-J.; Lemaux, S.; Demazeau, G.; Kim, J.-Y.; Choy, J.-H. *J. Am. Chem. Soc.* **2001**, *123*, 10413.
- (16) Krämer, G.; Jansen, M. *J. Solid State Chem.* **1995**, *114*, 206.
- (17) Krämer, G.; Hägele, E.; Wagner, N.; Jansen, M. *Z. Anorg. Allg. Chem.* **1996**, *622*, 1027.
- (18) Chen, B.-H.; Walker, D.; Scott, B. A. *Chem. Mater.* **1997**, *9*, 1700.
- (19) Hansen, T.; Müller-Buschbaum, Hk. *Z. Anorg. Allg. Chem.* **1992**, *616*, 67.
- (20) Panin, R. V.; Khasanova, N. R.; Bougerol, C.; Schnelle, W.; Van Tendeloo, G.; Antipov, E. V. *Inorg. Chem.* **2010**, *49*, 1295.
- (21) Tanaka, M.; Katsuya, Y.; Yamamoto, A. *Rev. Sci. Instrum.* **2008**, *79*, 075106.
- (22) Izumi, F.; Ikeda, T. *Mater. Sci. Forum* **2000**, 321–324, 198.
- (23) Bain, G. A.; Berry, J. F. *J. Chem. Educ.* **2008**, *85*, 532.
- (24) Werner, P.-E.; Eriksson, L.; Westdahl, M. *J. Appl. Crystallogr.* **1985**, *18*, 367.
- (25) LeBail, A.; Duroy, H.; Fourquet, J. L. *Mater. Res. Bull.* **1988**, *23*, 447.
- (26) Altomare, A.; Burla, M. C.; Camalli, M.; Carrozzini, B.; Cascarano, G. L.; Giacovazzo, C.; Guagliardi, A.; Moliterni, A. G. G.; Polidori, G.; Rizzi, R. *J. Appl. Crystallogr.* **1999**, *32*, 339.
- (27) Tancret, N.; Obbade, S.; Bettahar, N.; Abraham, F. *J. Solid State Chem.* **1996**, *124*, 309.
- (28) Obbade, S.; Tancret, N.; Abraham, F.; Suard, E. *J. Solid State Chem.* **2002**, *166*, 58.
- (29) Brese, R. E.; O'Keeffe, M. *Acta Crystallogr., Sect. B* **1991**, *47*, 192.
- (30) Brown, I. D. *Chem. Rev.* **2009**, *109*, 6858.
- (31) Krämer, G.; Jansen, M. *J. Solid State Chem.* **1995**, *118*, 247.
- (32) Inaguma, Y.; Tanaka, K.; Tsuchiya, T.; Mori, D.; Katsumata, T.; Ohba, T.; Hiraki, K.; Takahashi, T.; Saitoh, H. *J. Am. Chem. Soc.* **2011**, *133*, 16920.
- (33) Azuma, M.; Chen, W. T.; Seki, H.; Czapski, M.; Smirnova, O.; Oka, K.; Mizumaki, M.; Watanuki, T.; Ishimatsu, N.; Kawamura, N.; Ishiwata, S.; Tucker, M. G.; Shimakawa, Y.; Attfield, J. P. *Nat. Commun.* **2011**, *2*, 347.
- (34) Cox, D. E.; Sleight, A. W. *Solid State Commun.* **1976**, *19*, 969.
- (35) Arblaster, J. W. *Platinum Metals Rev.* **1994**, *38*, 119.